

# Seeing Galaxies Through Thick and Thin: II. Direct Measures of Extinction in Spiral Disks Through Spectroscopy of Overlapping Galaxies

Donovan L. Domingue, William C. Keel<sup>1</sup> & Raymond E. White III<sup>1</sup>

Department of Physics and Astronomy, University of Alabama, Box 870324, Tuscaloosa, AL 35487-0324; Electronic mail: domingue@hera.astr.ua.edu, keel@bildad.astr.ua.edu, white@merkin.astr.ua.edu

Received \_\_\_\_\_; accepted \_\_\_\_\_

---

<sup>1</sup>Visiting astronomer, Kitt Peak National Observatory, National Optical Astronomy Observatories, Operated by AURA, Inc. under cooperative agreement with the NSF.

## ABSTRACT

We use slit spectroscopy of overlapping pairs of galaxies to directly determine the extinction in disks of foreground spiral galaxies. The Doppler shifts of pair members are determined via cross-correlation and their relative correlation amplitudes are used to separate their contributions to the combined spectra in regions of overlap. This spectroscopic approach is less subject to stringent symmetry constraints than our previous purely photometric analyses. Extinctions of foreground members were obtained for 6 of the candidates in our sample of 18 mostly spiral/spiral pairs, when the signal to noise and velocity difference were suitable. In agreement with our previous imaging results, we find that the extinction in interarm regions is very modest, typically  $A_B \sim 0.1$  mag (corrected to face on), while spiral arms exhibit higher extinctions of  $\sim 0.3$  mag.

*Subject headings:* galaxies: spiral — galaxies: ISM — galaxies: photometry — galaxies: distances and redshifts

## 1. Introduction

Determining the opacity of spiral galaxy disks is essential to understanding how the dust content in disks can affect luminosity estimates, star formation rates, and the ability to see through these disks when observing distant objects such as QSOs. The inclination–surface-brightness test is one of the oldest methods (Holmberg 1958) used to determine whether spiral galaxies are largely transparent or opaque: opaque disks have surface brightnesses independent of inclination, while transparent disks are brightest when seen edge-on. A more refined version of this test used by Valentijn (1990) led to the claim that spiral galaxies are opaque. This result seems contrary to examples of objects seen through spiral disks and the fact that we are able to observe galaxies by looking beyond the Milky Way. Reassessments of Valentijn’s (1990) work by Burstein et al. (1995) and Huizinga (1994) have shown that sample selection effects can mask any relationship between inclination and surface brightness.

White & Keel (1992) initiated a campaign to determine *directly* (rather than statistically) the opacity of spiral disks by imaging partially overlapping galaxies. The non-overlapping parts of the galaxies in such systems are used to estimate how much light from the background galaxies is absorbed in passing through the foreground galaxies (White & Keel 1992; Keel & White 1995; White, Keel & Conselice 1996, 1999). The success of this differential photometric technique is strongly dependent on the symmetry of each of the overlapping galaxies, since the errors in the deduced optical depths are dominated by systematic errors due to deviations from structural symmetry.

In our photometric analysis, the symmetry requirements for both background and foreground components of a pair limits the number of useful pairs from our observed sample (White, Keel & Conselice 1999). Taking spectra of the overlap regions allows the symmetry requirements for the foreground galaxy to be relaxed, since we can directly

identify photon ownership, due to the velocity difference between the two galaxies. A Fourier cross-correlation of the spectra shows peaks at the velocities corresponding to the redshifts of each of the pair members. The relative Fourier amplitudes of the two peaks should be equivalent to the relative intensities of the foreground and background galaxies in the overlapping region. This velocity decomposition, combined with photometry of a symmetric background galaxy region, gives us an estimate of the foreground disk opacity. Here we present new opacity measurements using this technique for arm and interarm regions in six spiral galaxies. The relaxed symmetry requirements for the foreground galaxy allow us to analyze spirals which are not grand design.

## 2. Method Formalism

We first describe the differential photometric technique employed in our previous imaging studies, in order to contrast it with the present spectroscopic study. A partially overlapping pair of galaxies is illustrated in Figure 1. In the region of overlap, the surface brightness of the foreground galaxy is  $F$  and the unattenuated surface brightness of the background galaxy is  $B$ . Light from the background galaxy is attenuated while passing through the foreground galaxy, so what is actually observed in the overlap region is  $\langle F + Be^{-\tau} \rangle$ , where  $\tau$  is the optical depth in the foreground galaxy and the angle brackets are used to emphasize that the enclosed quantity is the basic observable. We use symmetric regions of both the foreground and background galaxies to *estimate*  $F$  and  $B$  in the overlap region, since we cannot directly decompose them with imaging; the estimates of  $F$  and  $B$  are denoted  $F'$  and  $B'$ . We then use purely differential photometry to derive an estimate of  $\tau$ , denoted  $\tau'$ :

$$e^{-\tau'} = \frac{\langle F + Be^{-\tau} \rangle - F'}{B'}. \quad (1)$$

That is, the estimate of the foreground light in the overlap region is first subtracted from the total light in the overlap region; the result is then divided by the estimate of unattenuated background light to derive an estimate of  $e^{-\tau}$ .

In contrast, our spectroscopic technique is illustrated in Figure 2, where a slit is seen crossing the overlap region and intersecting both galactic centers. In this case, if the radial velocity difference between the two galaxies is large enough, the foreground light  $F$  and the attenuated background light  $\langle Be^{-\tau} \rangle$  can be spectroscopically distinguished in the overlap region, in contrast to the purely photometric case above. In this case, all we need is an estimate  $B'$  of the *unattenuated* background galaxy's surface brightness  $B$ , derived from a symmetric region of the background galaxy. Our estimate of  $\tau$  in the overlap region can then be deduced with a modified version of equation (1):

$$e^{-\tau'} = \frac{\langle Be^{-\tau} \rangle}{B'}, \quad (2)$$

since  $F$  and  $\langle Be^{-\tau} \rangle$  are spectroscopically separable. We require only global symmetry in this case since  $B$  and  $B'$  may be averaged over substantial areas along the slit.

Puxley and James (1993) also exploited velocity separation of galaxy pairs in this context, using emission lines from HII regions. Our use of stellar *absorption* lines offers important advantages. The background continuum is smoothly distributed across large regions. Thus, we are not subject to point to point variations in opacity and are not biased against high opacity regions.

The cross-correlation method as applied will use all absorption features in our wavelength range (3600-5200 Å) of the template and galaxy spectra. This has the advantage of using lines blended by galaxy velocity dispersions in addition to easily identifiable lines. When they are taken into account, those blended lines may contribute the most signal to the cross-correlation. The combined spectra of two galaxies in the overlap region is compared to our templates. The absorption features of the individual galaxies contribute to

the correlation with differing strength due to their intensity levels. The brightest spectrum of the two will dominate and be most easily correlated, thereby producing the largest peak at its respective redshift.

### 3. Observations and Data Analysis

To explore how well Doppler separation of the light from the foreground and background galaxies would allow us to measure the extinction in overlapping pairs, we obtained optical spectra of 18 such pairs (see Table 1) using the 2.1m telescope and GoldCam spectrometer at Kitt Peak National Observatory in 1995 November. We concentrated on the line-rich spectral region from 3600-5200 Å, with the full spectral range falling on the  $3072 \times 512$ -pixel useful region of the Ford CCD, set comfortably wider than this (3100-6800 Å) so that defocusing at the ends of each spectrum would not compromise our cross-correlation results. The slit width of  $150\mu$  ( $1''.9$ ) gave a resolution of 4.1 Å (FWHM) with pixels subtending  $0''.78$  by 1.25 Å. A slit length of  $5'.0$  gave clear sky around the pairs to permit sky-subtraction for all members of the sample but NGC 4567/8. Most objects received total exposures of 120 minutes, intended to give usable count rates within at least the overlap region as a whole and, in several cases, for several independent bins within this region. Each object exposure was immediately followed by one of a HeNeAr comparison lamp, so that an individual wavelength solution could be generated for each observation. The rms deviation of comparison-line wavelengths about the adopted solution was typically 0.14 Å, so that the contribution of the calibration step to radial-velocity errors would be typically less than  $10 \text{ km s}^{-1}$ . Vignetting along the slit was measured and removed through an observation of the twilight-sky zenith. The velocity zero point was confirmed through nightly observations of the IAU radial-velocity standard stars BD +28° 3402 (F7 V,  $-36.6 \text{ km s}^{-1}$ ), HD 213947 (K4 III,  $+16.7 \text{ km s}^{-1}$ ), or HD 90861 (K2 III,  $+36.3 \text{ km s}^{-1}$ ). We also observed M32 at the

start of the run, as an additional cross-correlation reference.

Supporting *B* and *I* images for most of these pairs are available from the CTIO 1.5m, KPNO 2.1m, or Lowell 1.1m telescopes (as described by White, Keel, & Conselice 1998). For two systems in which the slit position did not cross the nuclei, we obtained an additional brief spectrum of the nuclei, to verify the systemic radial velocity of each galaxy.

Each sky-subtracted spectrum in our sample was cleaned using IRAF to get rid of cosmic rays and remove columns where sky lines did not subtract well. Removal of pixel columns at wavelengths greater than 6500 Å was done to remove poor data. Since the line-rich region contributing most of the cross-correlation power is below 5200 Å, no interesting information was lost. Averages were taken in the spatial direction across galaxy nuclei and turned into one dimensional spectra. The 1-D spectra were cross-correlated, using the IRAF task FXCOR, with the radial velocity standard spectra to get redshift estimates and determine which standards worked best for each galaxy. The spectra of M32 and HD213947 were determined to be the most useful references but BD +28° 3402 was also used as a check on velocity estimates. After the galaxies with previously known redshifts were shown to agree with our estimates, heliocentric redshifts were obtained for the galaxies with unpublished radial velocities.

To analyze the area of combined spectra, the overlap region was located in angular distance from the galaxy nuclei along the position angle of the slit. Extracted spectra were usually the sum of four detector pixels (3''1) along the slit, to increase the signal to noise. Whenever possible, adjacent regions overlapped each other by two pixels. These 1-D spectra were cross-correlated with the radial velocity standards and double peaked profiles were sought near the respective velocities of the pair members. When a correlation proved unsuccessful, the sizes of the 1-D spectra were reevaluated and summed over a smaller region until results were achieved or options were exhausted. Final region selections are

shown in Figures 5 through 11.

If observed cross-correlation peaks were located at the expected redshifts, their relative amplitudes were compared. Averages of relative amplitudes from correlations with two different standards were calculated when possible. The relative amplitudes were taken as the fraction of foreground to background light. Association of the peaks with the position of galaxies was determined by matching velocities, since foreground and background contributions switched dominance as a function of distance from the respective nuclei. In one pair, NGC 7268, the foreground galaxy has a higher recession velocity than that of the background galaxy by  $\sim 400 \text{ km s}^{-1}$ . It is interesting to note that in our first clean photometric case, AM1316-241, the recession velocity of the foreground galaxy exceeded that of the background galaxy by an even greater amount,  $\sim 700 \text{ km s}^{-1}$  (White & Keel 1992).

Once the fractional foreground contribution was determined, two methods were used to estimate the fluxes from symmetric areas of the background galaxy. First, when the slit encompassed the necessary symmetric background region, the galaxies' spectra were averaged over all wavelengths to create an intensity profile of the pair. The intensities in the symmetric background regions in the slit were then estimated to produce opacity measures as described above. Second, we used images of the pairs to estimate the unabsorbed contribution of the background galaxy from symmetric, nonoverlapping regions. This method is a hybrid of our purely photometric and our purely spectroscopic techniques. When we use both methods, we refer to the purely spectroscopic technique as the spectral method and the hybrid as the spectrum/image method.

The velocity per pixel resolution of our spectra proved to be a limiting factor in obtaining double velocity peaks in the cross-correlations. Since most of the galaxies differed in velocity by less than  $\sim 300 \text{ km s}^{-1}$ , the peak with lower correlation amplitude could



be located within the span of the higher amplitude peak. A higher spectral dispersion would produce greater separation in the peaks. This blending was usually the reason why a candidate pair failed to yield opacity measures. In some cases the orientation of the galaxy disks produced an advantageous increase in velocity separation at the regions of interest which allowed measures to be made for NGC 1738/9 despite the pair’s relative velocity. Other failures were due to obtrusive emission lines in the desired region of the spectra or to low signal to noise. The role of signal to noise was investigated with synthetic composite spectra having varying S/N ratios. Decreasing the signal to noise in a spectra with two equal correlation amplitudes at a separation of  $500 \text{ km s}^{-1}$  made distinguishing peaks more difficult while the lowest ratios caused FXCOR to be unable to find any peaks at the proper locations.

Metallicity effects among the galaxy pair members were found to be unimportant since the depth of absorption lines is not as important as their placement with respect to the template spectrum. Our templates from the spectra HD213947, a K star, and M32 with a K star dominated spectrum show metallicity differences by way of line depths. Both of these templates were used in the cross-correlations and the very similar results were averaged and reported. An increased relative line depth would improve the correlation if it were large enough to stand out in a noise filled spectrum, so our signal to noise ratio is a larger concern to achieve results. The two galaxies of largest morphological difference in our useful sample are the members of the NGC 7268 pair. Using FXCOR to cross-correlate non-overlapping portions of this pair with one template reveals the same level of correlation for an SBbc and an S0, therefore metallicity effects are ignored. Since we also observe the non-overlapping portions of the galaxies within the spectroscopic slit, we are only sensitive to possible asymmetries in line strengths.

We used synthetic composite spectra to calibrate the mapping between ratios of

Fourier amplitudes to foreground/background intensity ratios. We found that the mapping of this ratio from real space to Fourier space is dependent on the velocity resolution of the input spectra. Artificial spectra with different redshifts were created with MK1DSPEC and combined with known relative contributions of background and foreground light. The resulting cross-correlation amplitudes were then compared to the input intensity ratios. Artificial spectra were created with a velocity resolution comparable to that of our real data, which have  $75 \text{ km s}^{-1} \text{ pixel}^{-1}$ . The test Fourier amplitude ratios of the two peaks were found to be within 10% of the input intensity ratios, independent of the value of the ratio. Figure 4 plots the input continuum ratio against that inferred from FXCOR for the  $75 \text{ km s}^{-1} \text{ pixel}^{-1}$  tests with various velocity space separations. Nearly all observed amplitude ratios are between 1 and 2, with only two regions greater than 3, so the expected errors from the Fourier measure should all fall near 5%. Similar tests were performed by shifting the spectrum of M32 to two different velocities and combining them into one spectrum. Those results show that correlation amplitude blending for separations of less than  $500 \text{ km s}^{-1}$  causes ratios to be less accurate as is also shown in Figure 4. With this analysis, pairs still fall within an acceptable 10% error. These effects are smaller than our measurement errors so we do not apply corrections.

#### 4. Results

Individual galaxy pairs which gave useful opacity measurements are discussed below. The extinctions are reported in magnitudes, where the relation between magnitudes of extinction  $A$  and optical depth  $\tau$  is  $A=1.086\tau$ . Our measured values correspond roughly to  $A_B$ , since most of the strong absorption features giving cross-correlation signal lie in the  $B$  band. Other pairs in our sample lack discernible double peaks in the collected spectral cross-correlations. Table 2 contains a summary of properties of the seven pairs

with useful results followed by those galaxies which did not yield results; the redshifts listed are those calculated with FXCOR unless otherwise noted. All morphological types,  $R/R_{25}^B$  values, and noted redshifts were obtained from the NASA/IPAC Extragalactic Database (NED), the ESO-LV catalog (Lauberts & Valentijn 1989), or the RC3 (de Vaucouleurs et al. 1991). Table 3 lists the face-on corrected extinctions, along with corresponding regions and averages. Negative extinction values in the table indicate the level of systematic error due to departures from symmetry in the associated background galaxies.

#### 4.1. ESO 054642-2534.4

ESO 054642-2534.4 is comprised of two SBs in the cluster AM 0546-253 (see Figure 5) and is our most easily distinguished spectral pair, due their approximate velocity separation of  $1300 \text{ km s}^{-1}$ . Results were obtained for four regions with a two pixel wide overlap, corresponding to  $1''.56$  of shared width. These regions span nearly 2.5 kpc, using the galaxy redshift distance ( $H_0 = 75 \text{ km s}^{-1} \text{ Mpc}^{-1}$ ). The four areas sweep across a background arm/ring and a foreground arm/ring. The spectral intensity profile method yields an average extinction of  $A_B \approx 0.25$ , ranging from 0.08 to 0.48; the  $B$  image/spectrum method yields an average  $A_B \approx 0.11$ . Face-on corrected values are 0.17 and 0.07 for the two methods, respectively, after dividing by the axial ratio  $a/b = 1.47$ . Interarm material in the foreground galaxy is revealed to have average extinctions of  $A_B = 0.2$  and 0.15 through inspection of three of the regions using the two methods defined above.

#### 4.2. ESO 064906-3517.3

In ESO 064906-3517.3, an Sa-Sab pair, we found three regions which give double peaked cross-correlations (see Figure 6). These regions are four pixels ( $3''.1$ ) wide and span

an area including some foreground spiral arm. The foreground and background galaxies contribute comparable amounts of light in each region. Extinctions average to  $A_B = 0.18$  using the spectrum intensity profile method. These data imply a face-on value of  $A_B = 0.11$ , assuming a simple cosine inclination dependence and the observed foreground galaxy axial ratio  $a/b = 1.61$ . Face-on values for the regions identified as being in a foreground arm average to be  $A_B = 0.15$ .

### 4.3. MCG -02-58-011

MCG -02-58-011 is comprised of an edge-on foreground SBc, oriented E-W, projected against a highly inclined blue late-type spiral, oriented N-S. Reddened knots are seen in the disk oriented E-W only in the overlap region; these knots are otherwise similar to those in the disk oriented N-S, which leads to the conclusion that the edge-on E-W SBc is in the foreground. We found six regions with discernible light contributions from both pair members (see Figure 7); these regions are four pixels wide and each shares two pixels. Unfortunately, these regions have no unobscured symmetric counterparts, so we cannot accurately estimate opacities. We can merely state that the foreground member is not completely opaque.

### 4.4. NGC 1738/9

NGC 1738/9 comprises an SBbc-Sbc pair for which our single spectroscopic slit position did not pass through background areas symmetric to our regions of interest (see Figure 8), due to geometric constraints. We were however able to estimate opacities despite the velocity separation being less than  $100 \text{ km s}^{-1}$ . Cross-correlation of spectra from the overlap region proved to be easiest with the nuclear spectrum of NGC 1738. In combination with

the  $B$  image/spectrum method, three one pixel (0.2 kpc) wide regions reveal an average apparent  $A_B = 0.76$  for these arm regions. Dividing by the axial ratio of the foreground galaxy NGC 1739 ( $a/b = 1.95$ ) yields a face-on corrected value of  $A_B = 0.39$ , which is in general agreement with our previous photometric analysis of this pair (White, Keel, & Conselice 1998).

#### 4.5. NGC 3088

NGC 3088 consists of a nearly face-on foreground S0 projected against a background, nearly edge-on spiral galaxy. We found four useful regions that are four pixels ( $3''.1$ ) wide and share a width of two pixels with their neighbors (see Figure 9). Expected asymmetries in an edge-on spiral complicate measurements for this pair. Negative values indicate that some obscured regions behind the S0 have a greater brightness than geometrically symmetric regions in the background member. Although the negative values are unphysical, they are presented here and in Figures 12-14 for completeness. The S0 has average disk extinctions of  $A_B = 0.15$  using the spectrum method and  $A_B = -0.30$  using the spectrum/image method. Face-on-corrected values are 0.13 and -0.27, respectively, given an axial ratio of 1.12.

#### 4.6. NGC 6365

The NGC 6365 pair consists of a nearly edge-on Sdm (NGC 6365B) projected against a SBcd galaxy (see Figure 10). We analyzed five regions, each one pixel wide, lying along NGC 6365B. The apparent extinctions derived from this spectrum method indicate that NGC 6365B is the foreground galaxy which agrees with the respective redshifts, however the decision is complicated by a region on NGC 6365B that appears diminished in brightness

by a possible arm of the face-on member. In contrast there appears to be an arm of NGC6365A peeking from behind the edge-on member. The interpretation, that NGC 6365B is the foreground, is favored for meaningful extinctions. Because of spectral similarities, a cross-correlation with the NGC 1739 spectrum was most useful. The foreground galaxy has average face-on corrected interarm extinctions of  $A_B = 0.15$  and  $0.17$ , for the spectrum and spectrum/image methods, respectively (and an axial ratio of  $a/b = 3.70$ ).

#### 4.7. NGC 7268

The galaxy pair associated with NGC 7268 (see Figure 11) has a foreground SB ringed galaxy with a recession velocity  $400 \text{ km s}^{-1}$  greater than that of the background S0/E galaxy. Results were obtained for two regions, each  $1''.56$  ( $\sim 1 \text{ kpc}$ ) wide and not sharing any pixels. The location of these areas with respect to galaxy features appears to be in the outer ring of the foreground barred galaxy. The average ring extinctions are  $A_B = 0.53$  (using the intensity profile method) and  $A_B = 0.30$  (using the  $B$  image/spectrum method). The face-on corrected values are  $A_B = 0.35$  and  $A_B = 0.21$ , given an axial ratio of  $a/b = 1.50$ .

### 5. Summary and Discussion

We have used slit spectroscopy of overlapping pairs of galaxies to determine directly the extinction in foreground spiral disks. Our spectroscopic technique allows us to relax the symmetry requirements of our previous imaging studies. In agreement with our previous imaging results, we find that the extinction in interarm regions is typically  $\sim 0.1 \text{ mag}$  in blue (corrected to face on), while spiral arms exhibit extinctions of  $\sim 0.3 \text{ mag}$ . In this sample, rings exhibit the same level of extinction as spiral arms. These numbers are calculated as an average of both methods used in this paper. Face-on extinctions are

estimated by dividing by axial ratios and therefore can be overestimates since realistic cases have finite thickness and clumped absorbers. The values obtained can be expected to have errors of at least 5% due to cross-correlation uncertainties but values will be most affected by unwanted asymmetry in the background light comparisons.

A plot of uncorrected extinctions as a function of axial ratio (Fig. 12), for data obtained in this paper and from White, Keel, & Conselice (1999), reveals a great deal of scatter amongst arm regions. This comparison reveals no inclination dependence in the apparent extinctions. The separation of arm and interarm values is clear. A similar comparison of face-on extinctions with galaxy type (Fig. 13) also reveals scattering of values for spiral arms and a more consistent measurement for the interarm regions. The individual internal structures of galaxies may play an important role in the scatter. In Figure 14, extinctions as a function of  $R/R_{25}^B$  are plotted and show a suggestion of decreasing values with increasing radius for interarm regions while arm region extinctions show no dependence on radius. The outlying points at the lower left are from the S0 galaxy, NGC 3088 which has a possibly asymmetric edge-on galaxy in the background.

This spectral decomposition technique is a viable way of determining disk opacities. As discussed by White, Keel, & Conselice (1999), these results suggest that galaxy extinction is not the cause of the QSO “cutoff” and that intrinsic galactic luminosities are not as underestimated as they would be if spirals were completely opaque.

This research has made use of the NASA/IPAC Extragalactic Database (NED) which is operated by the Jet Propulsion Laboratory, California Institute of Technology, under contract with the National Aeronautics and Space Administration. This research has also made use of *SKYVIEW*. D.D. thanks Guy Purcell and Victor Andersen for helpful technical support. We thank Paul Eskridge for observing NGC 3088 and NGC 6365 with the 1.3 meter MDM.

## REFERENCES

- Burstein, D., Haynes, M. P., & Faber, S. M. 1991, *Nature*, 353, 515
- Burstein, D., Willick, J., & Courteau, S. 1995, in *The Opacity of Spiral Disks*, eds. J.I. Davies & D. Burstein, (Dordrecht: Kluwer), p.73
- de Vaucouleurs, G. et al. 1991, *Third Reference Catalog of Bright Galaxies*, Springer-Verlag
- Holmberg, E. 1958, *Medd. Lunds Astr. Obs*, ser 2, no. 136
- Huizinga, J. E. 1994, Ph.D. thesis, Rijksuniversiteit Groningen
- James, P. A., & Puxley, P. J. 1993, *Nature*, 363, 240
- Keel, W. C. & White, R. E. III 1995, in *The Opacity of Spiral Disks*, eds. J.I. Davies & D. Burstein, (Dordrecht: Kluwer), p.167
- Lauberts, A. & Valentijn, E. A. 1989, *The Surface Photometry Catalogue of the ESO-Uppsala Galaxies*, European Southern Observatory
- Valentijn, E. A. 1990, *Nature*, 346, 153
- White, R. E. III & Keel, W. C. 1992, *Nature*, 359, 129
- White, R. E. III, Keel, W.C. & Conselice, C. J. 1996, in *New Extragalactic Perspectives in the New South Africa*, ed. D. Block & M. Greenberg, (Dordrecht: Kluwer), p. 114.
- White, R. E. III, Keel, W. C., & Conselice, C. J. 1999, *ApJ*, in press



## Figure Captions

Fig. 1.— Schematic of differential photometric technique for estimating extinction in a foreground spiral of a partially overlapping pair of galaxies.

Fig. 2.— Schematic of spectroscopic technique for estimating extinction in a foreground spiral of a partially overlapping pair of galaxies.

Fig. 3.— Sample cross-correlation results from FXCOR can be seen to exhibit two separate peaks near the Gaussian fit. They are located at the respective redshifts of the galaxies and the peak heights represents the intensity contributions of the pair members.

Fig. 4.— Plot of estimated accuracy for foreground/background light contributions obtained from FXCOR for synthetic spectra and M32 spectra with  $\sim 75 \text{ km s}^{-1} \text{ pixel}^{-1}$  velocity resolution. Various velocity separations are plotted.

Fig. 5.— *B* band image of ESO 054642-2534.4 with placement of spectroscopic slit illustrated along with the four numbered areas in Table 3. The regions are approaching a resonance ring but are primarily composed of interarm material. Regions are not shown to overlap for purposes of clarity.

Fig. 6.— Digitized Sky Survey image of ESO 064906-3517.3 with placement of spectroscopic slit illustrated along with the three regions crossing a spiral arm numbered as in Table 3. Regions are not shown to overlap for purposes of clarity.

Fig. 7.— *B* band image of MCG -02-58-011 with placement of spectroscopic slit illustrated along with the six numbered areas in Table 3. The regions surround the nucleus of the vertical galaxy which is possibly the background member. They are located such that symmetric counterparts are represented by the regions opposite the nucleus and prevent reasonable estimates of the extinction. Regions are not shown to overlap for purposes of clarity.

Fig. 8.— *B* band image of NGC 1738/9 with placement of spectroscopic slit illustrated along with the three numbered areas in Table 3. These regions are in a spiral arm of NGC 1739 which can be seen cutting out the light of NGC 1738.

Fig. 9.— *B* band image of NGC 3088 with placement of spectroscopic slit illustrated along with the four numbered areas in Table 3. The regions are near the edge of the S0. Regions are not shown to overlap for purposes of clarity.

Fig. 10.— *B* band image of NGC 6365 with placement of spectroscopic slit illustrated along with the five numbered areas in Table 3. The regions surround the disk of the inclined galaxy.

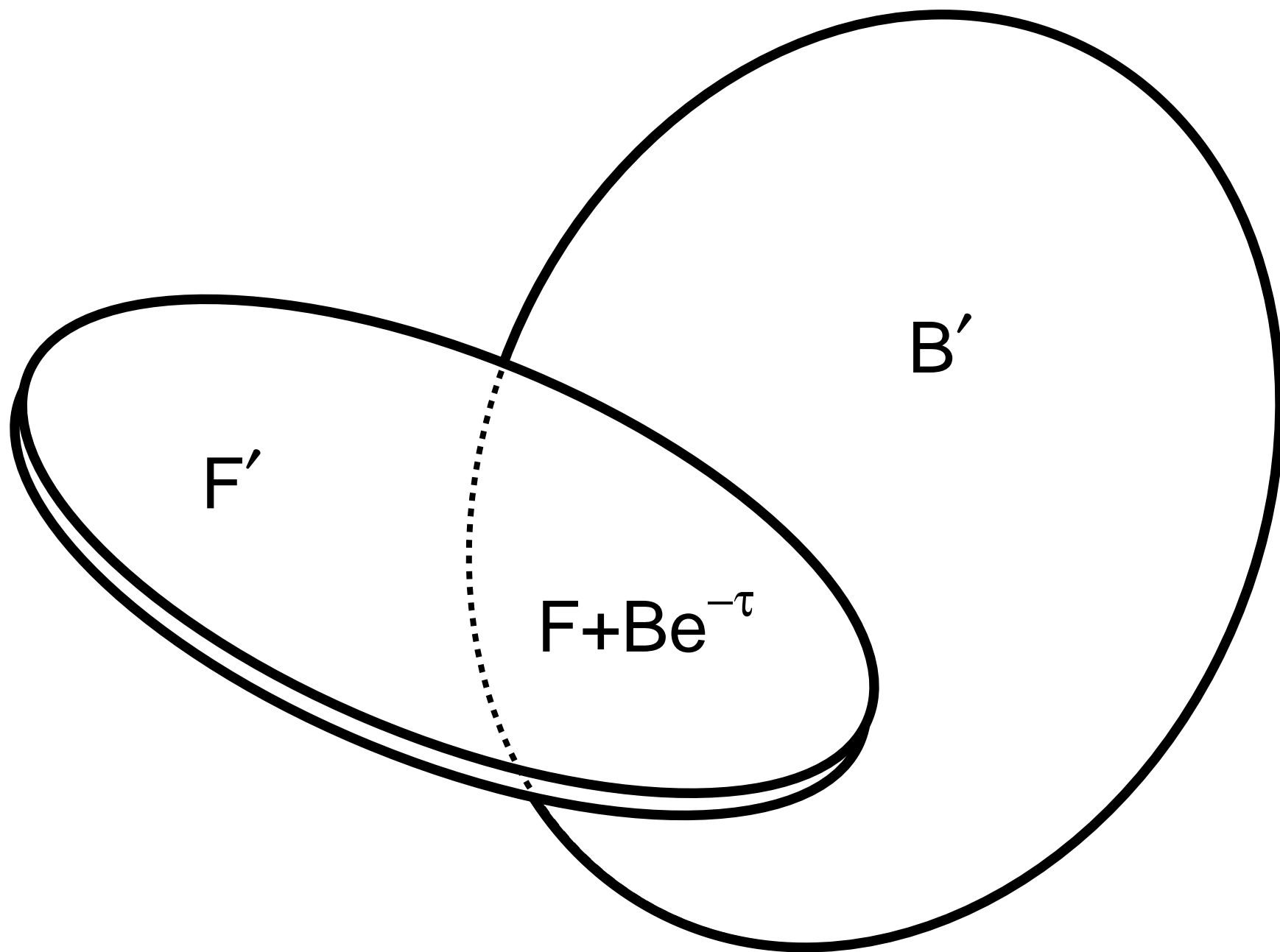
Fig. 11.— *B* band image of NGC 7268 with placement of spectroscopic slit illustrated along with the two numbered areas in Table 3. The regions are in a dusty resonance ring of the foreground galaxy. Regions are not shown to overlap for purposes of clarity.

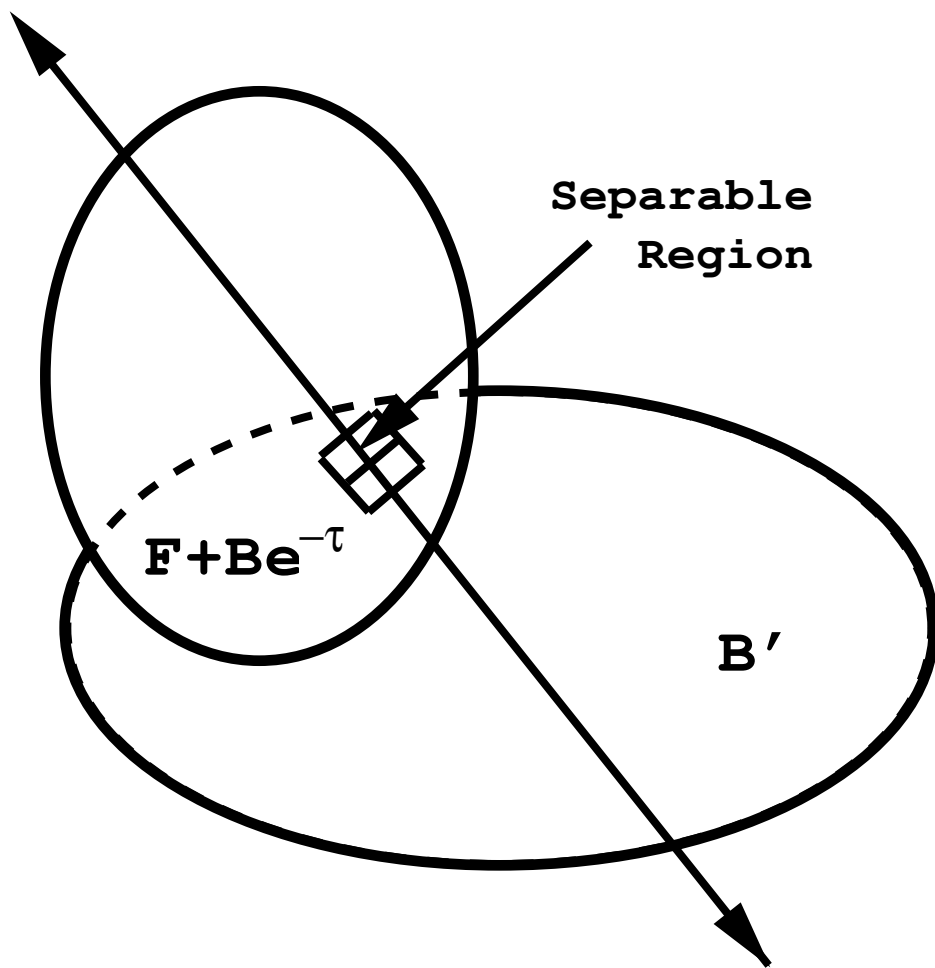
Fig. 12.— Plot of apparent extinction as a function of axial ratio ( $a/b$ ) for the ensemble of galaxies reported on as well as those from White, Keel, & Conselice (1999). Filled circles represent the sum of arm regions for each galaxy and open circles represent the sum of interarm regions. NGC 3088 is represented by plus signs in all figures.

Fig. 13.— Plot of face-on-corrected extinction as a function of galaxy type for the ensemble of galaxies reported on as well as those from White, Keel, & Conselice (1999). Filled circles represent the sum of arm regions for each galaxy and open circles represent the sum of interarm regions.

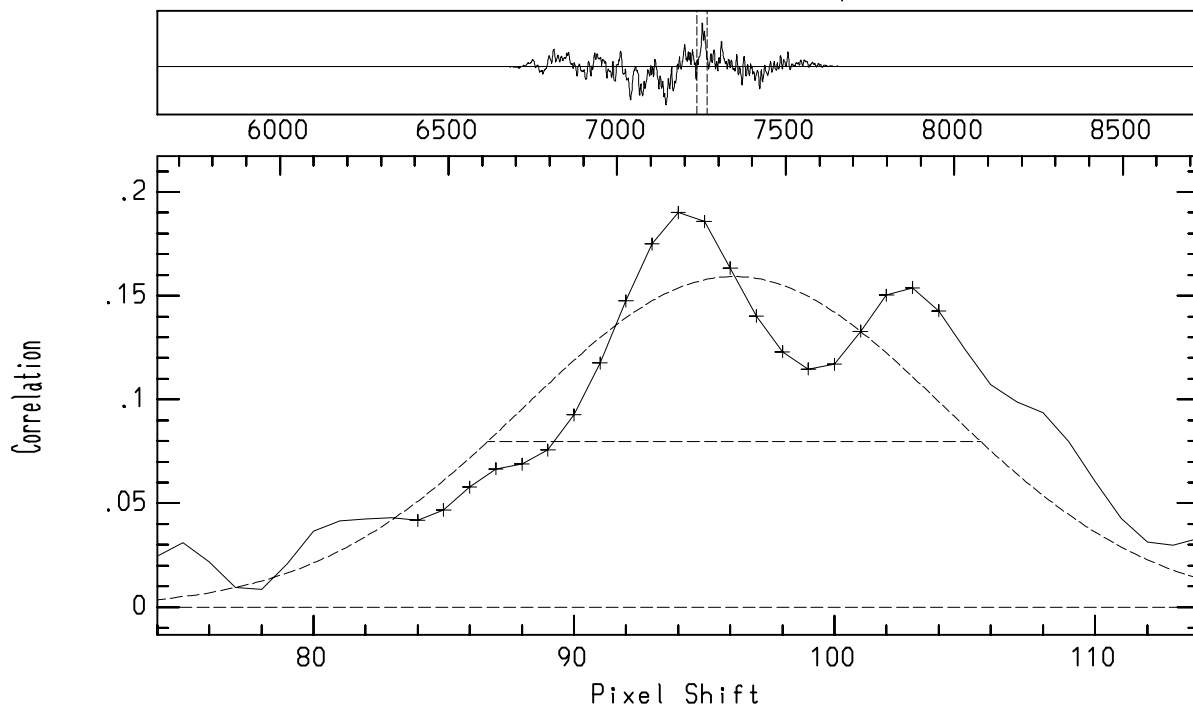
Fig. 14.— Plot of face-on-corrected extinction as a function of the ratio of radius to de Vaucouleurs radius for the ensemble of observed galaxy regions reported on as well as those from White, Keel, & Conselice (1999). Filled circles represent arm regions and open

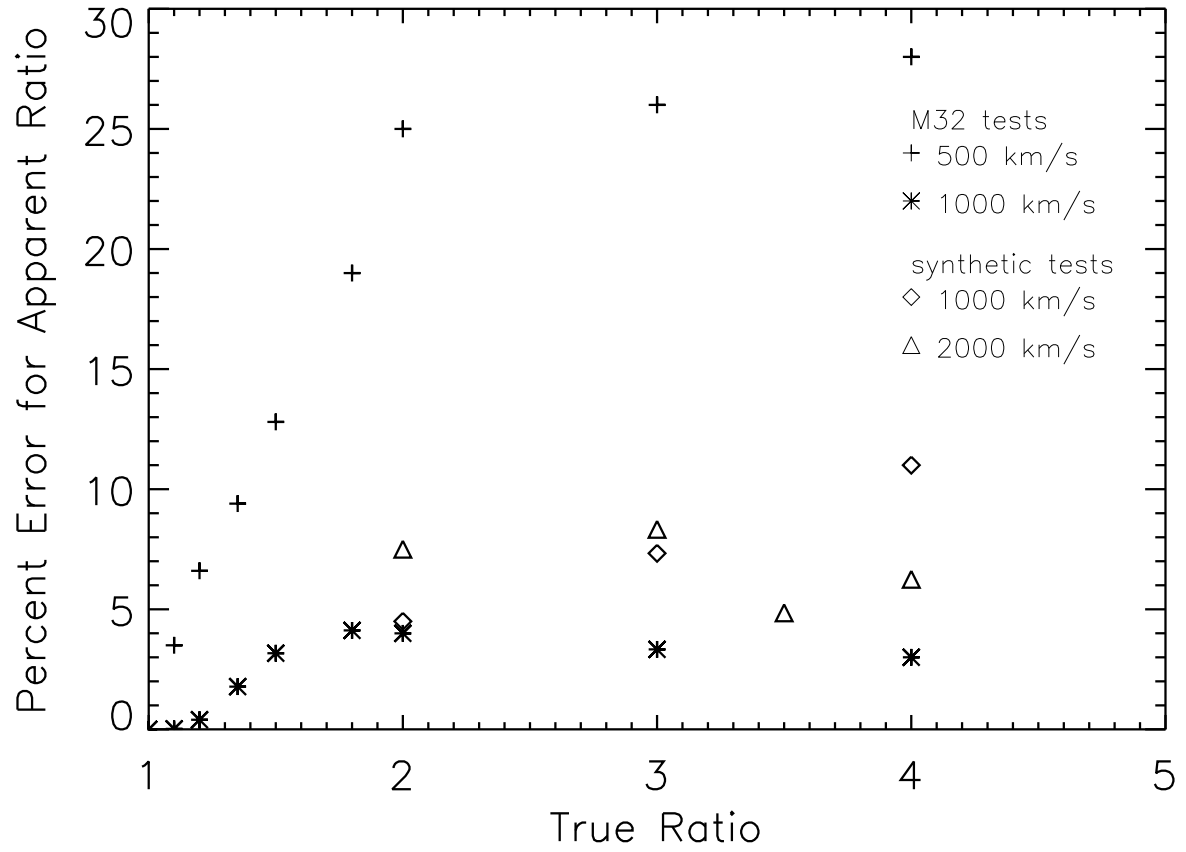
circles represent the interarm regions. The plus signs represent the regions from the NGC 3088 pair.

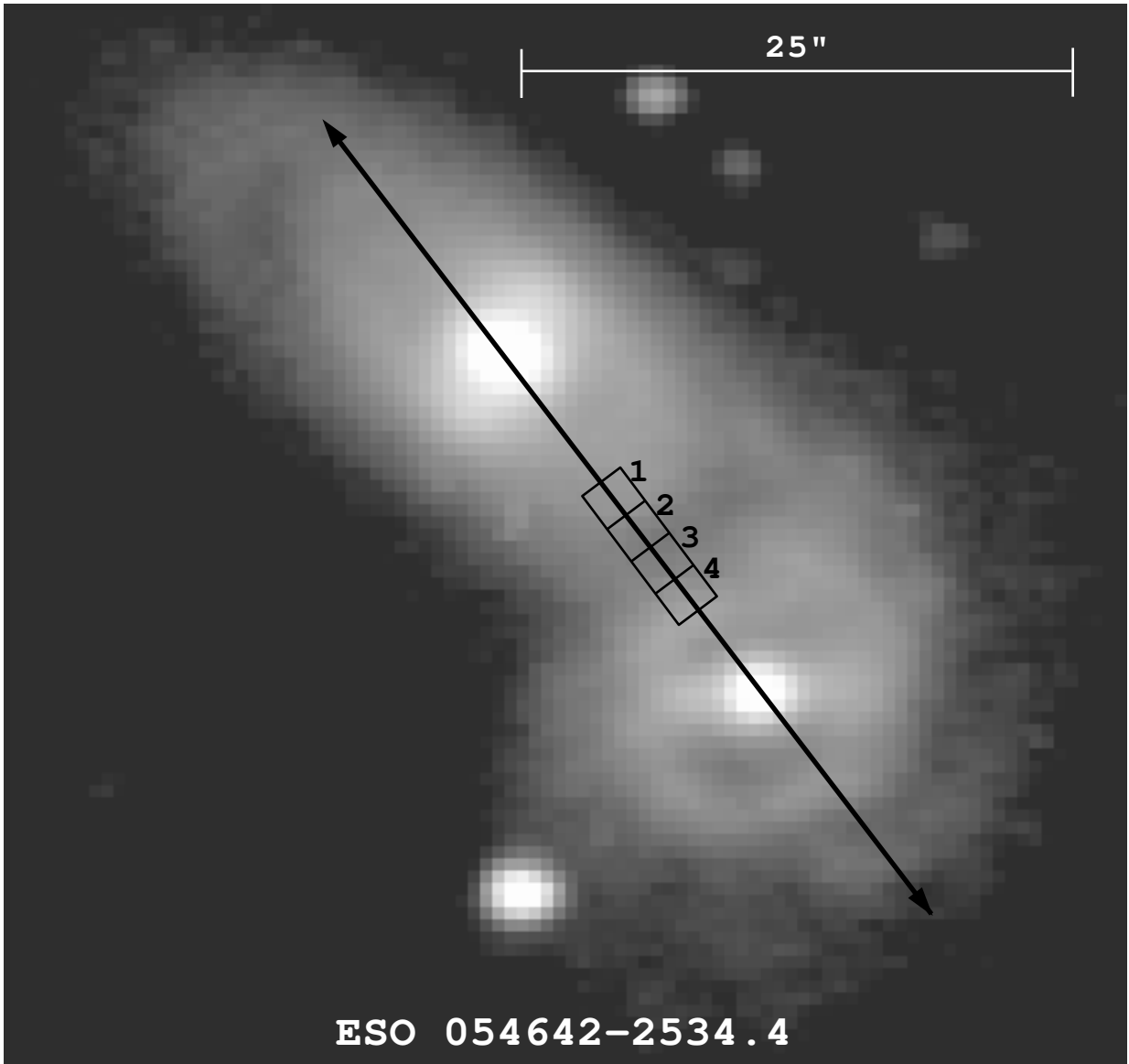




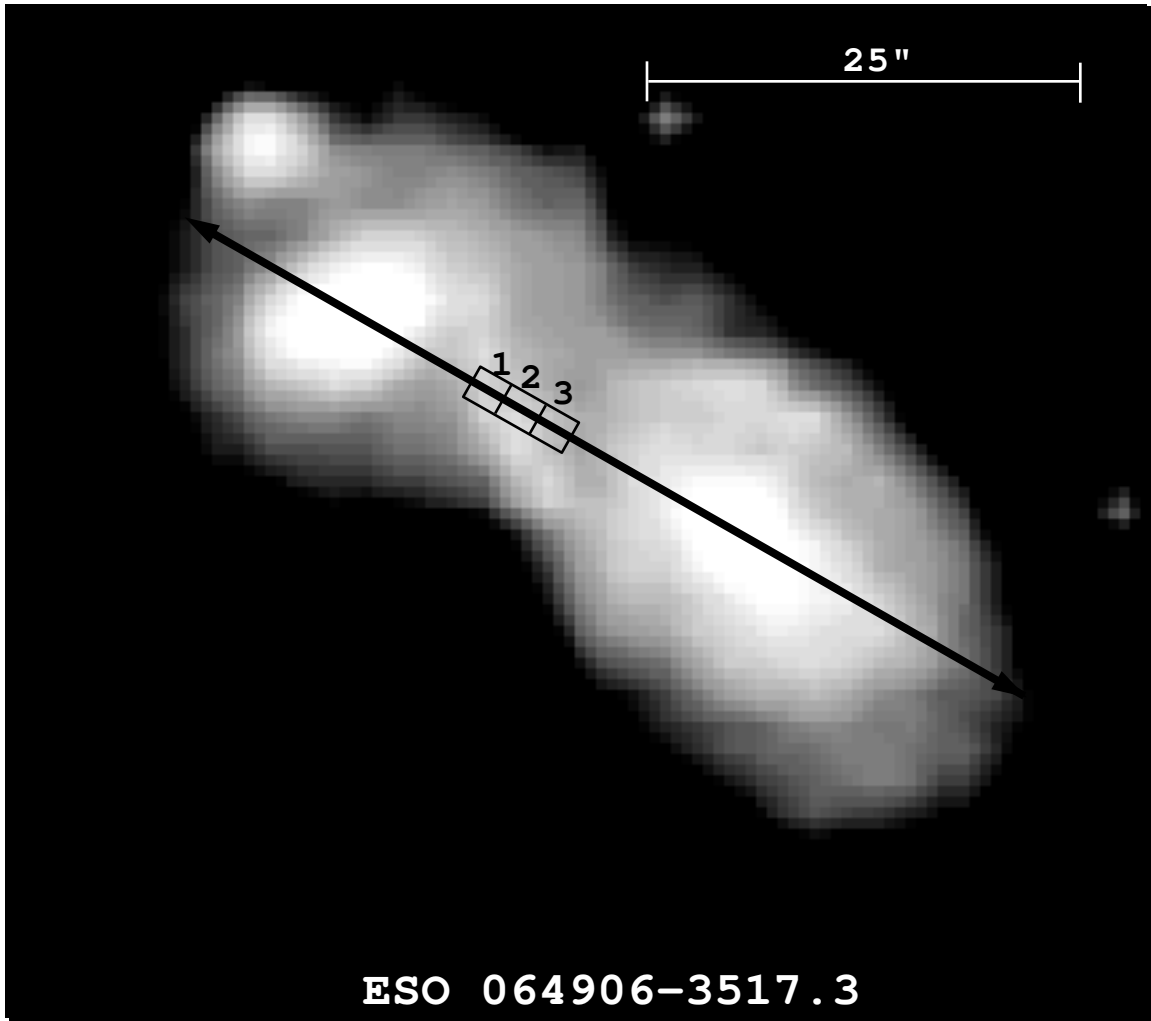
NOAO/IRAF V2.10.3BETA domingue@bama Fri 13:20:09 30-Jan-98  
Object='lp3088\_4' Temp='tgal1' npts=4096 aperture=209  
Star = 'UGC\_5384\_=\_NGC\_3088\_PA135' Template = 'M32\_PA0'

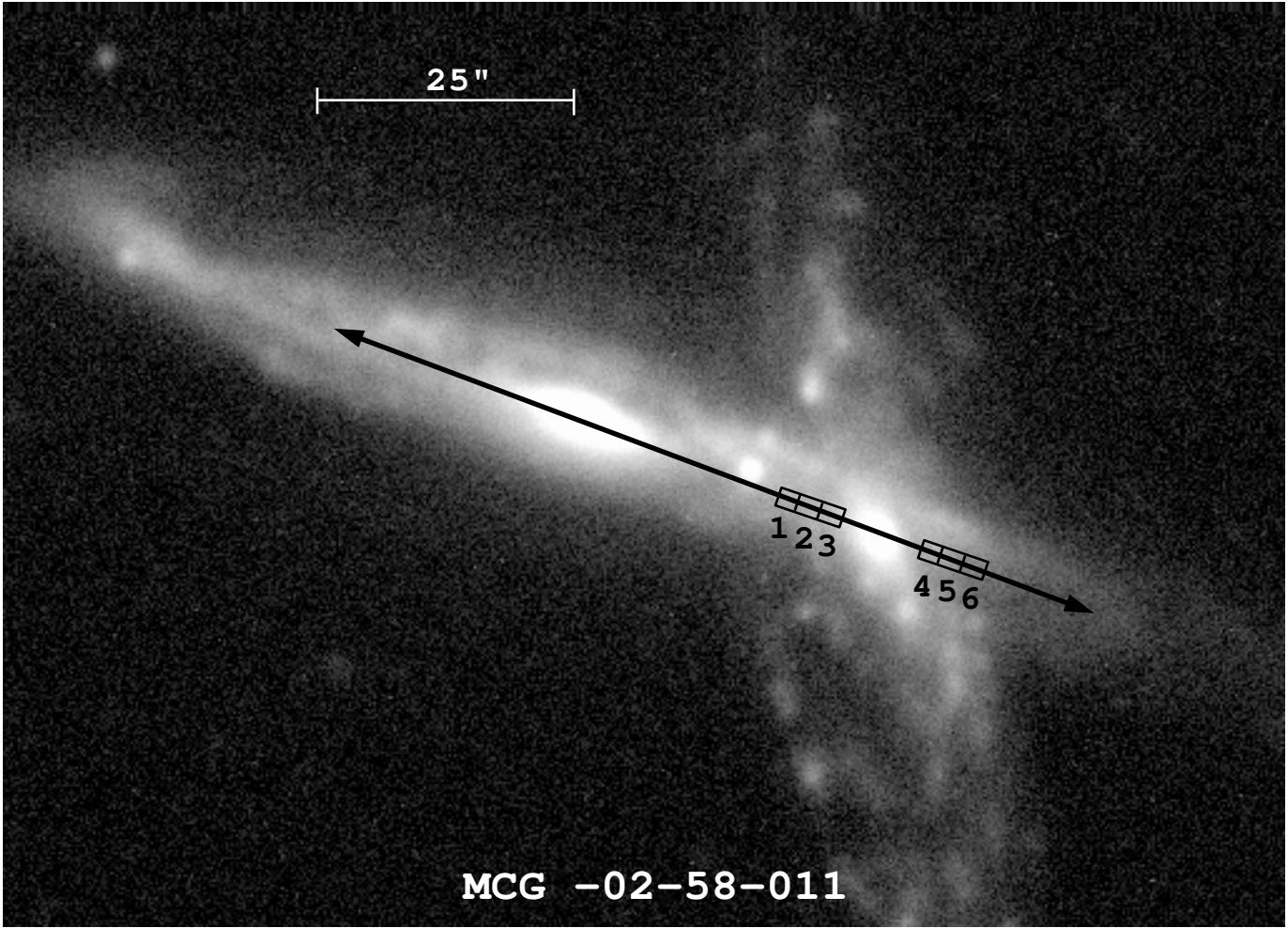


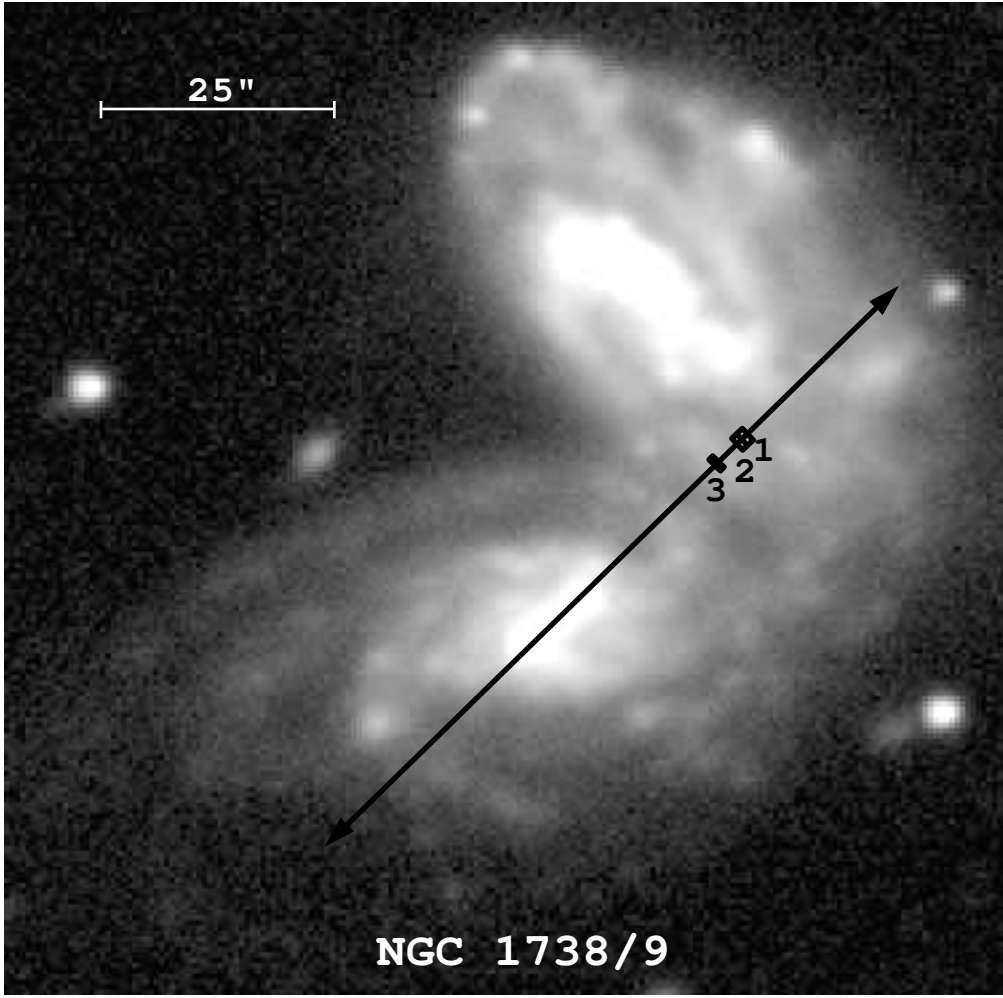


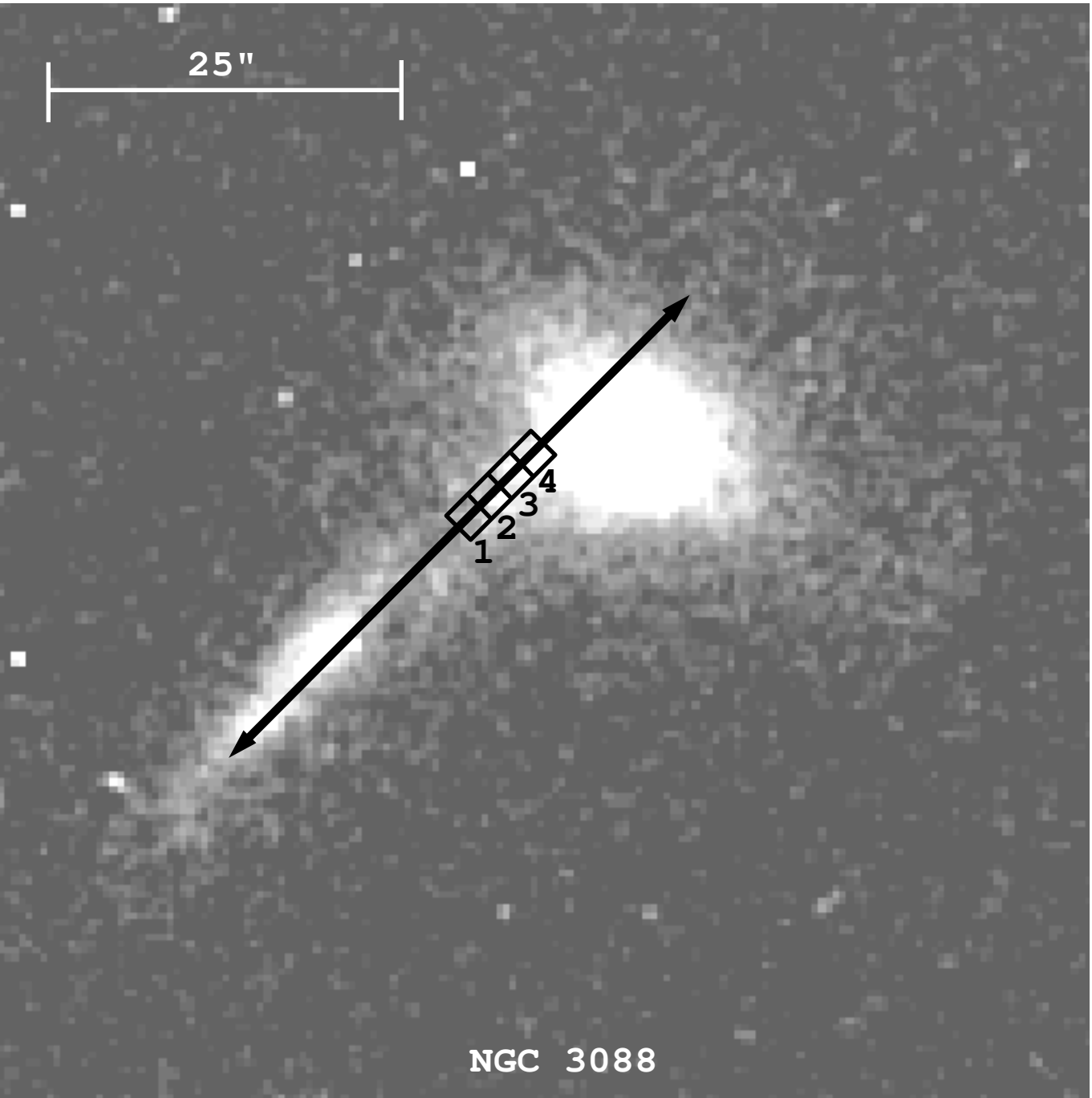


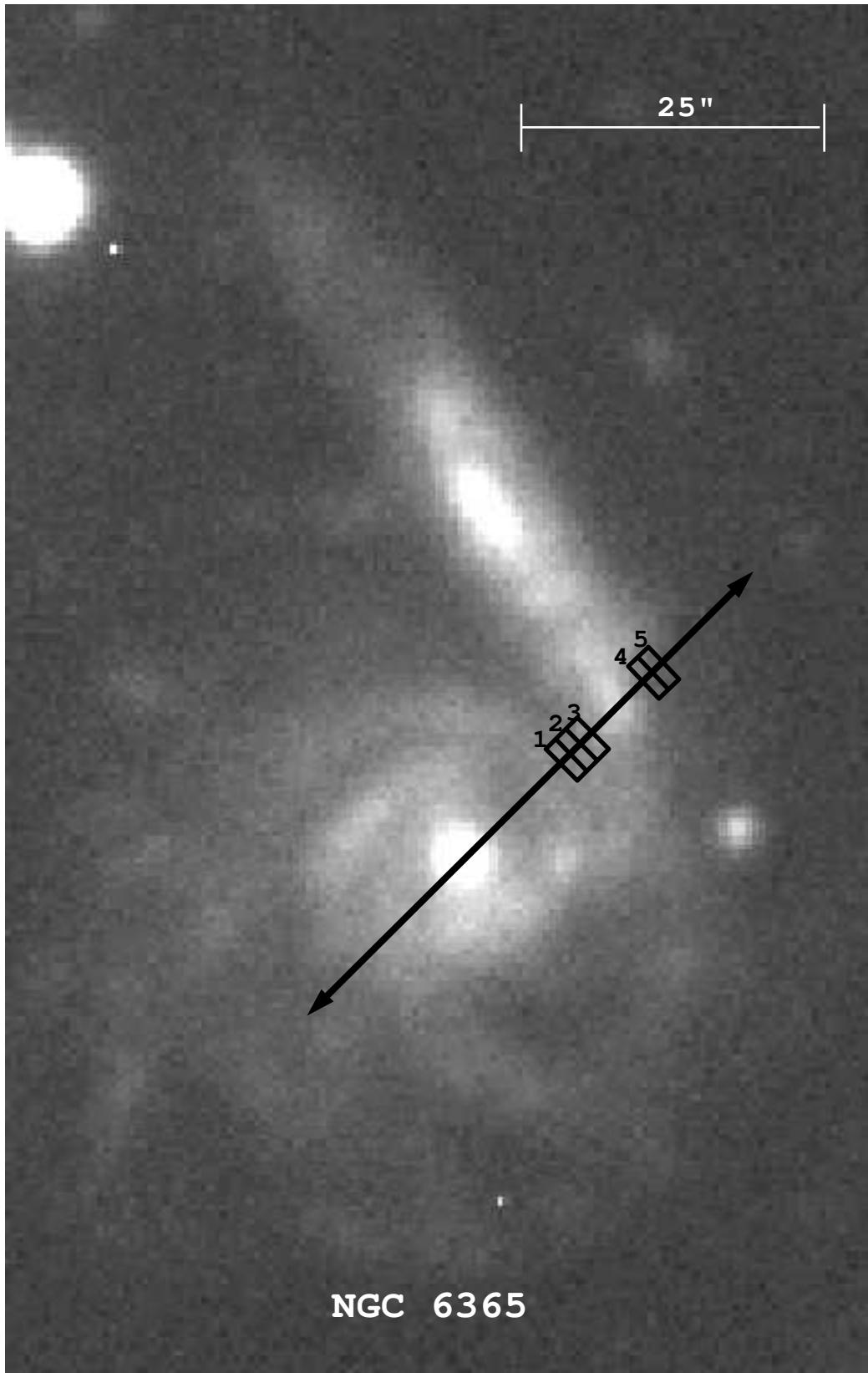






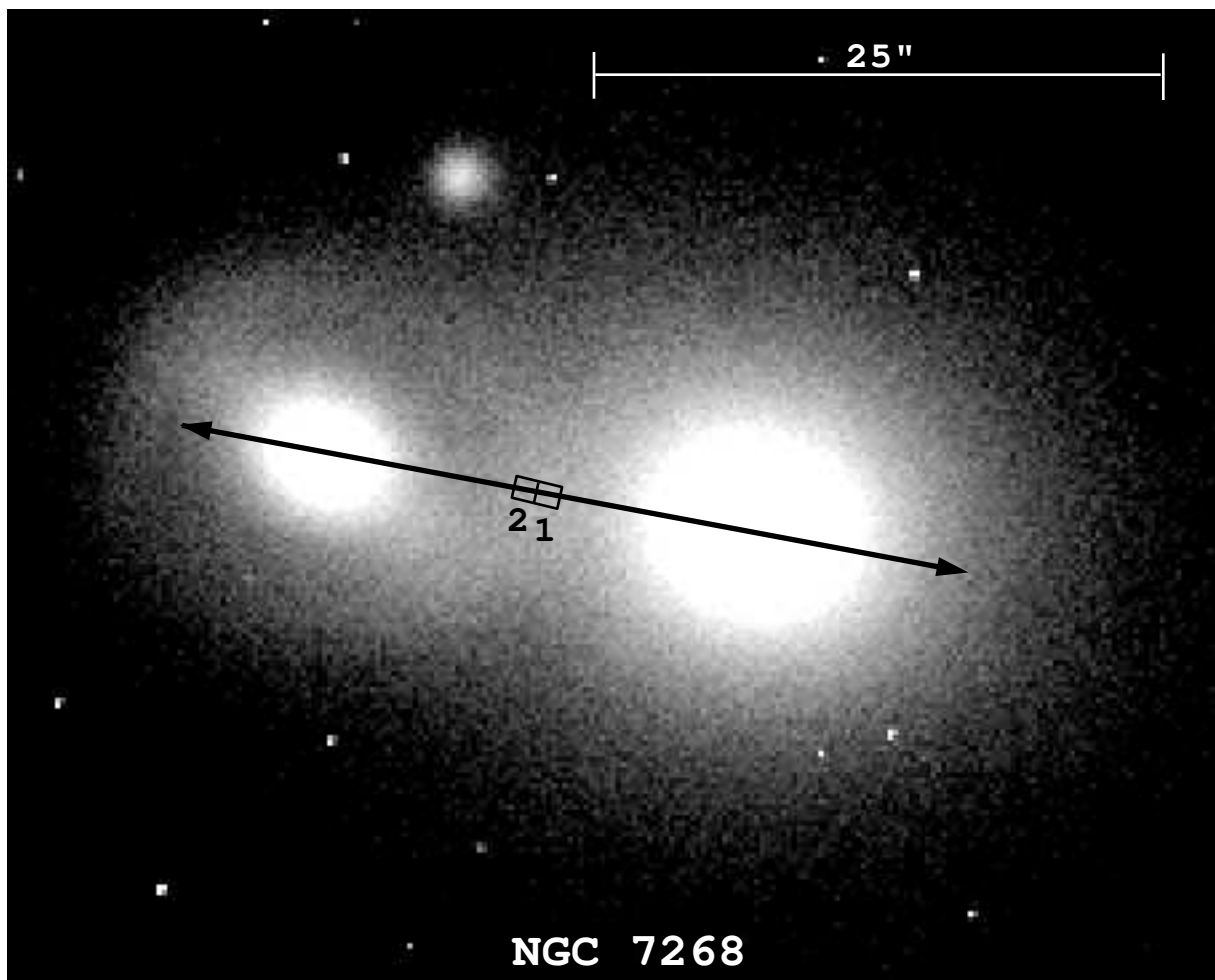


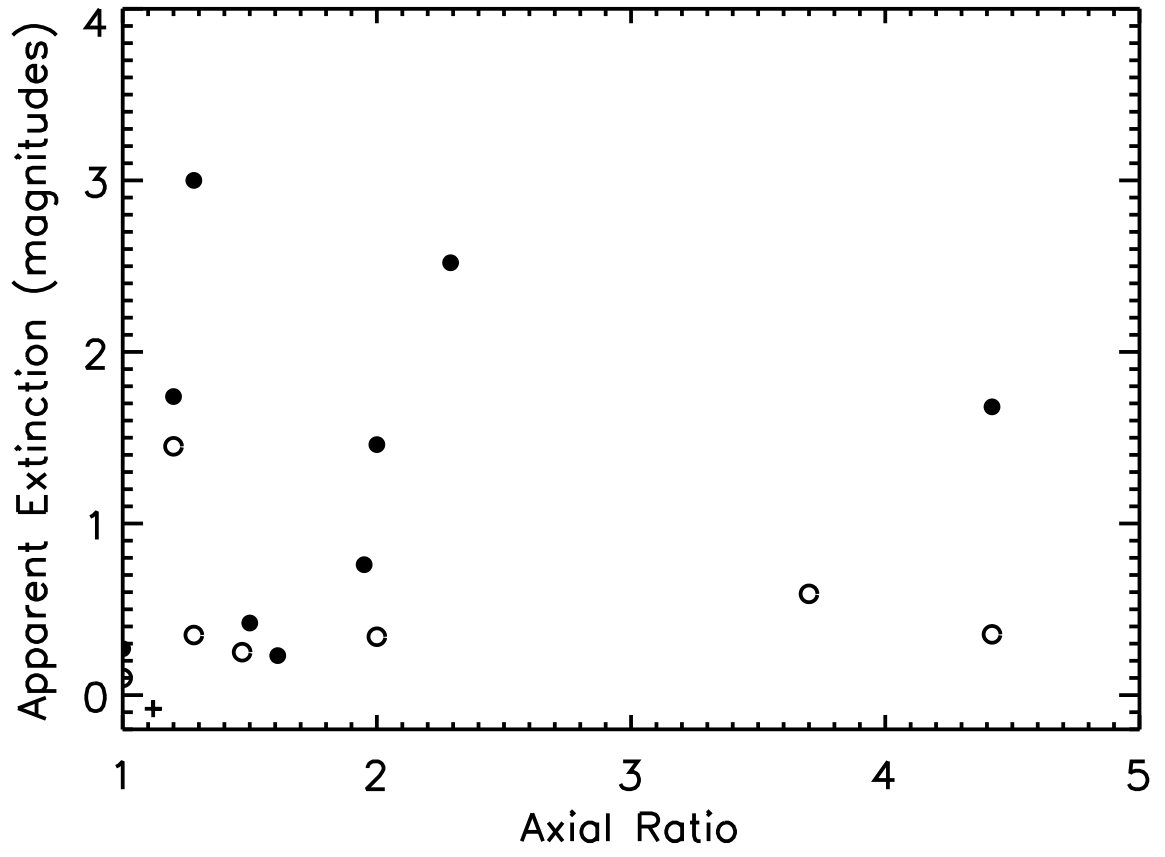


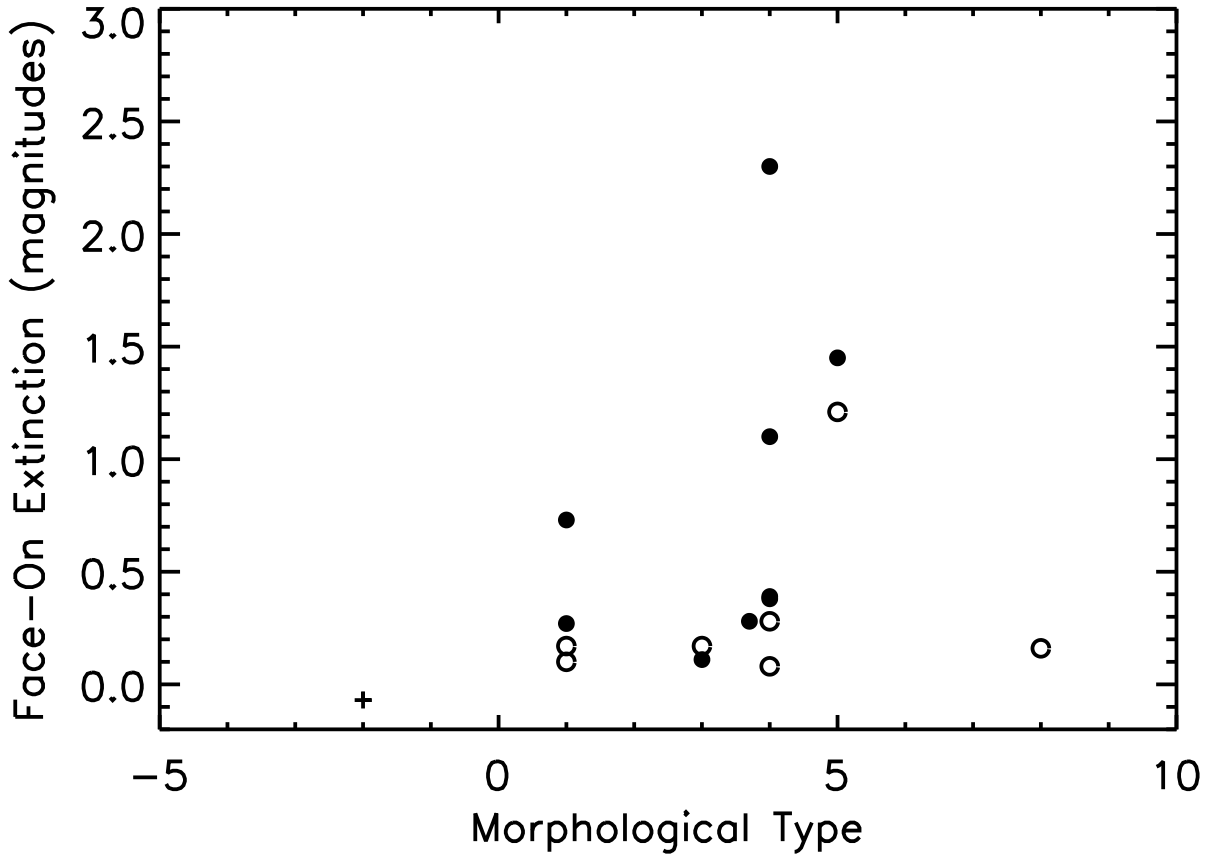


25"

NGC 6365









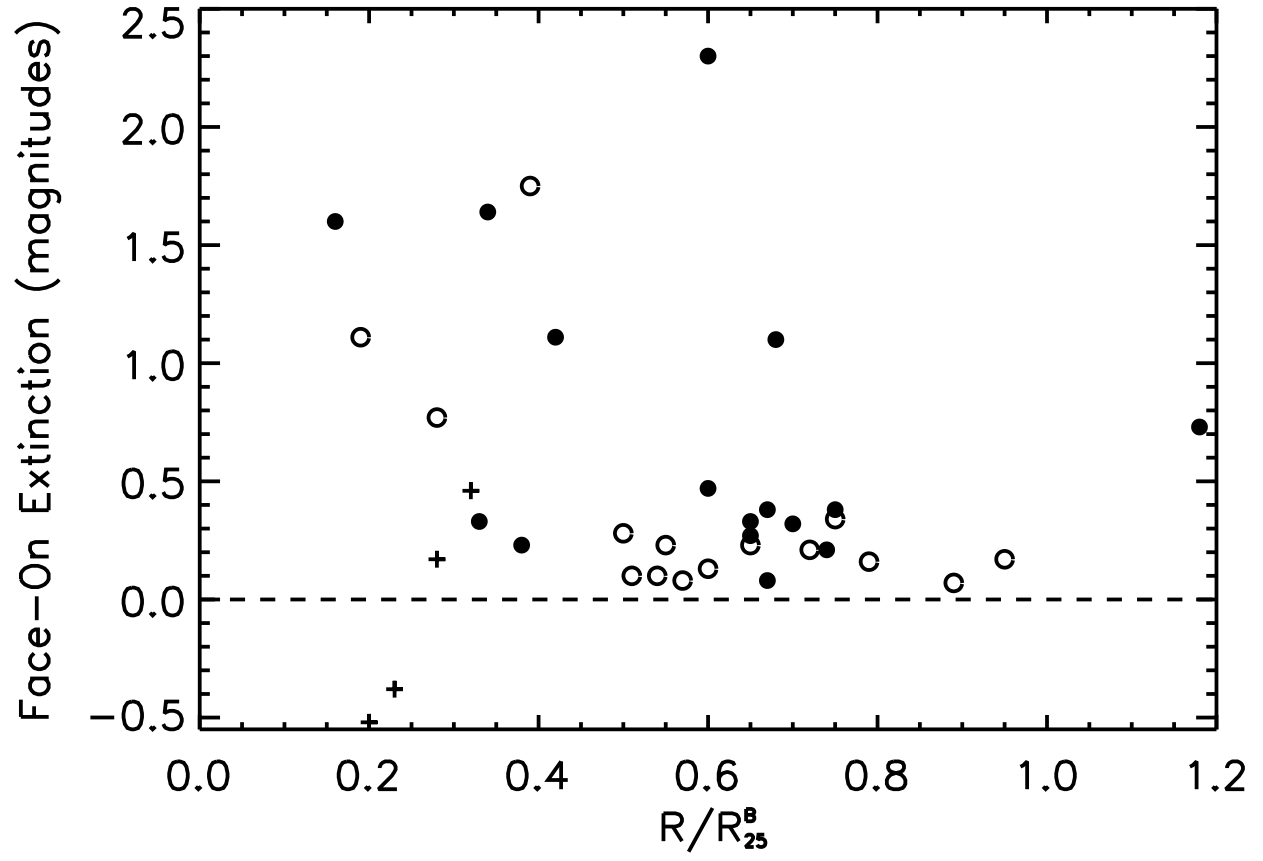


Table 1: Observations of Overlapping Pairs

Name	Position angle (degrees)	Total exposure (minutes)
AM 2354-304	110	60
Arp 198	57	60
CPG 41	164	120
ESO 054642-2534.4	37	120
ESO 064906-3517.3	62	85
IC 5364	83.5	120
MCG -02-58-011	71	120
NGC 190	-4	20
NGC 1738/9	60 & -46	60 & 120
NGC 1888/9	49	60
NGC 2207/IC 2163	97	60
NGC 3088	135	70
NGC 4567/8	103	90
NGC 6365	135	120 & 60
NGC 7268	80	90
NGC 7436	90	60
UGC 3445	94	45
UGC 3995	103	60

TABLE 2  
 PROPERTIES OF GALAXY PAIRS

Foreground <i>alternate name</i>	a/b	type	$R_{25}^B$ "	$cz^a$ (km/s)	Background <i>alternate name</i>	type	$cz^a$ (km/s)
ESO 054642-2534.4 eso-lv 4880291	1.47	SBb	16	$11000 \pm 85$	... eso-lv 4880290	SBab	$12373 \pm 16$
ESO 064906-3517.3 eso-lv 3660250	1.61	Sb	26	$9983 \pm 53$	... eso-lv 3660251	Sab	$10354 \pm 62$
MCG-02-58-011 VV 488	4.75	SBc	60	$4907 \pm 40$	...	S	$5148 \pm 91$
NGC 1739	1.95	SBbc	42	$3886 \pm 33$	NGC 1738	Sbc	$3978^b$
NGC 3088 MCG +04-24-010	1.15	S0	$39^c$	$7092 \pm 54$	... MCG +04-24-011	S	$7478 \pm 96$
NGC 6365B UGC 10833	3.7	Sdm	33	$7904^b$	NGC6365A UGC 10832	SBcd	$8518 \pm 51$
NGC 7268B eso-lv 4670571	1.5	SBbc	28	$8807 \pm 57$	NGC 7268A eso-lv 4670570	S0/E?	$8421 \pm 61$
AM 2354-304 MCG -05-01-012	1.7	Sb	...	$9198 \pm 47$	... MCG -05-01-013	Sb	$18404 \pm 71$
Arp 198 UGC 06073a	6.0	S	...	$8813 \pm 60$	... UGC 06073b	S?	$8851 \pm 83$
CPG 41A	1.5	SB	...	$8890 \pm 84$	CPG 41B	Sc	$9172 \pm 79$
IC 5364 MCG -05-01-008	1.0	E/S?	...	$8953 \pm 53$	... MCG -05-01-007	E+S0/S	$9217 \pm 52$
NGC 190 NED01	1.0	Sab	27	$12157 \pm 34$	NGC 190 NED02	E0	$12214 \pm 81$
NGC 1888	3.75	SBc	91	$2443 \pm 60$	NGC 1889	E+	$2487 \pm 28$
NGC 2207	1.54	SABbc	128	$2733 \pm 41$	IC 2163	SBc	$2771 \pm 48$
NGC 4568	2.3	SABc	137	$2255^b$	NGC 4567	SABc	$2275 \pm 34$
NGC 7436B MCG +04-54-006	1.0	E	60	$7340 \pm 99$	NGC 7436A MCG +04-54-005	S	$7668 \pm 65$
UGC 3445	3.5	S0/a	42	$3080 \pm 25$	UGC 3446	S0	$3119 \pm 49$
UGC 3995 comp		S?		$4762 \pm 73$	UGC 3995	Sb	$4793 \pm 46$

Table 3: Face-On-Corrected Galaxy Extinctions

Galaxy	Region	bg/fg <sup>a</sup>	Spectra $A$	Spectra/Image $A$	$R/R_{25}^B$	Description
ESO 054642-2534.4	1	3.91	0.09	0.04	0.89	interarm
	2	1.25	0.32	0.36	0.75	interarm
	3	0.96	0.20	0.06	0.60	interarm
	4	0.67	0.05	-0.17	0.45	ring-edge
	average	1.70	0.17	0.07	0.67	
ESO 064906-3517.3	1	1.04	0.21	...	0.74	arm
	2	1.00	0.08	...	0.67	arm
	3	0.93	0.04	...	0.62	arm-edge
	average	0.99	0.11	...	0.68	
MCG-02-58-011	1-6	3-8	...	...	0.34-0.64	arm/interarm
NGC 1739	1	1.01	...	0.32	0.70	arm
	2	1.04	...	0.38	0.67	arm
	3	1.12	...	0.47	0.60	arm
	average	1.06	...	0.39	0.66	
NGC 3088	1	0.75	0.56	0.35	0.32	interarm
	2	0.62	0.28	0.05	0.28	interarm
	3	0.54	0.00	-0.76	0.23	interarm
	4	0.50	-0.32	-0.71	0.20	interarm
	average	0.60	0.13	-0.27	0.26	
NGC 6365B	1	1.42	0.13	0.18	0.79	interarm
	2	0.78	0.19	0.23	0.72	interarm
	3	0.53	0.22	0.24	0.65	interarm
	4	0.52	0.09	0.10	0.51	interarm
	5	0.66	0.10	0.10	0.54	interarm
average	0.78	0.15	0.17	0.64		
NGC 7268B	1	0.91	0.32	0.14	0.38	ring
	2	1.07	0.38	0.27	0.33	ring
	average	0.99	0.35	0.21	0.36	

<sup>a</sup>Ratio of background to foreground light.